# Terahertz optical and electrical properties of hydrogen-functionalized carbon nanotubes

Chul Kang,[1,*] In Hee Maeng,[1] Seung Jae Oh,[1] Seong Chu Lim,[2] Kay Hyeok An,[2] Young Hee Lee,[2] and Joo-Hiuk Son[1,†]
[1]*Department of Physics, University of Seoul, Seoul 130-743, South Korea*
[2]*Department of Physics, Center for Nanotubes and Nanostructured Composites, Sungkyunkwan University, Suwon 440-756, South Korea*
(Received 22 June 2006; revised manuscript received 9 November 2006; published 7 February 2007)

This study characterized hydrogen-functionalized carbon nanotube films and compared their characteristics before and after they were hydrogen functionalized, using terahertz (THz) time-domain spectroscopy. Reduction of the power absorption of the samples was observed with hydrogen functionalization. To analyze the experimental results, the effective medium approximation (EMA) was adopted. Through the EMA, the effective plasma frequencies, damping rates, and other physical parameters located in the THz region were determined. In this way, decreases in the plasma frequencies and the damping rates were observed after hydrogen functionalization, which implies a decrease in the carrier density.

DOI: 10.1103/PhysRevB.75.085410 PACS number(s): 78.66.−w, 78.20.Ci, 78.30.Na

## INTRODUCTION

Since Iijima synthesized the carbon nanotube (CNT) in 1991, it has occupied an important position in the science and engineering fields.[1,2] CNTs have many potential applications in nanomechanical engineering, light-emitting sources, and nanoelectronic devices.[2–7]

The biggest impediment to its electronic device applications, however, is that its electrical properties cannot be conveniently controlled during the growth process, and as-grown CNTs have the compositions of both semiconducting and metallic CNTs and are contaminated with other catalysts. Thus, for the application of CNTs in nanoelectronics, modification of their electronic characteristics after growth is essential. To modulate the electrical and optical properties of CNTs, various postgrowth processes are utilized. For instance, gas vapor functionalization and the insertion of metallic particles in CNTs have been tried and resulted in the modulation of the band gap by up to a few eV.[8,9]

Gas-phase functionalization was shown to easily transform metallic CNTs to semiconducting ones simply through hydrogen exposure.[8] Exposing an individual CNT to atomic hydrogen generated C-H bonds on the surface of the CNT, which resulted in an increase in the $sp^3$ hybridization, which enhances the semiconducting characteristics of the CNT. The carrier transport dynamics that explains the semiconducting properties of CNTs has not been characterized, however, although transport parameters such as plasma frequency, damping rate, carrier density, and mobility are important in CNT application to the field of solid-state electronics. In addition, understanding of the collective CNT properties in networks and junctions is required.

Previously, Fourier-transformed infrared (FTIR) spectroscopy and microwave spectroscopy have been used in the study of the ac electrical properties of CNT films in the far IR region because the transport parameters are located in the terahertz (THz) frequency region.[10,11] However, the spectral range from a few hundred gigahertz to a few THz is inherently unstable because the power of electronic transport devices, including transistors and diodes, drops quickly with increasing frequency, whereas the transition devices of the optical source such as lasers deliver very low optical power below a few THz.[12,13] Therefore, these techniques cannot ensure a good signal-to-noise ratio. However, THz time-domain spectroscopy (TDS) has a signal-to-noise ratio of over 10 000:1 and has many other advantages over other ac and dc measurement methods such as FTIR and current-voltage (*IV*) measurements.[14–19] Moreover, it does not require preprocessing such as probe-line fabrication to acquire electrical signals, because it can measure without contact. The most important feature of THz TDS is that it can acquire phase information during the measurement due to the coherence of the THz electromagnetic wave source.

In this study, THz TDS was used to study the optical and ac electrical properties of hydrogenated CNTs in the 0.2–2.5 THz region. The experimental results were fitted using the effective medium approximation, including the Maxwell-Garnett and Bruggemann models. The fit yielded the transport parameters of plasma frequencies, damping rates, etc. of functionalized CNT networks.

## EXPERIMENT

For hydrogen functionalization, single-walled CNTs were prepared using the traditional arc discharge technique. To fabricate homogeneous CNT films, CNTs were sonicated for about 24 h in an isopropyl alcohol solution and sprayed on a $10\times20\times3$ mm$^3$ quartz substrate. The film was 17 $\mu$m thick. For the deoxidation, the sample was heated. The heating temperature was 600 °C, and the heating time was 30 min in an argon ambient.

The functionalization of the CNTs using hydrogen gas was performed in a vacuum chamber. The quartz substrate was located on a Mo plate, and a W wire was set above the film. The vacuum system was filled with hydrogen gas up to 1 torr. Then the W wire was heated using a dc current of 17 A for 30 s, and the temperature of the W wire was set at about 1700 °C.

To study the influence of hydrogenation, the general photoconductive THz TDS setup shown in Fig. 1 was used. The generation antenna were coplanar lines with a gap of 80 $\mu$m on a GaAs substrate, and the detection antenna was a Hertzian dipole antenna, which had a gap of 5 $\mu$m on low-temperature-grown (LT) GaAs. The lifetime of the LT GaAs

 

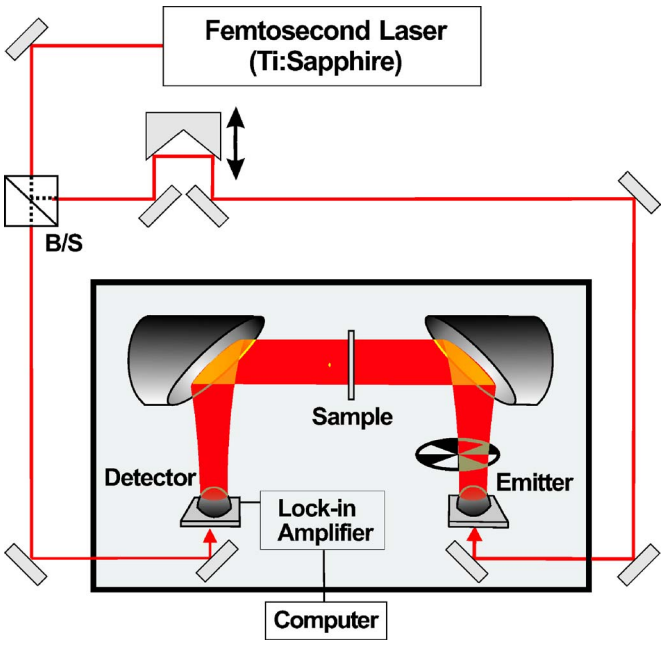


FIG. 1. (Color online) Scheme of the terahertz time-domain spectroscopy setup.

was about 250 fs. To collect the diverging THz beam, hemispherical silicon lenses with a resistivity of 10 kΩ/cm were mounted on the back of the generation and detection antennas. The samples were located between the paraboloids, where the THz beam was collinearly propagated through a pinhole. The pinhole size was 4 mm.

## RESULTS AND DISCUSSION

The reference and measured data in the time and frequency domains are shown in Fig. 2. In Fig. 2(a), the current amplitude of pristine CNTs was reduced to about half of that of the reference, which was the THz signal that passed only through the quartz substrate. Also, the current amplitude of hydrogen-functionalized CNTs was reduced to about two-fifths of the reference wave form in the time domain. Phase delays are also observed in the figure due to the passage of the signals through the samples. Figure 2(b) shows the normalized frequency-domain data. In the graph, although the spectral amplitudes of the reference data extend from 0.1 to 3 THz, the amplitude signal of the samples ranges from 0.2 to 2.5 THz as the THz pulses weakened at high frequencies due to the high absorption of CNTs. The spectral amplitudes of both samples showed similar reductions to the time-domain decrease, compared with those of the reference data.

Through the fast Fourier transformation of each datum, the spectral amplitude and the phase delay were acquired. Using the relationship described below, the power absorption and the refractive index were conveniently acquired:[14–16,19]

$$O(\omega) = I(\omega)\exp\left(-\frac{d\alpha(\omega)}{2}\right)\exp\left(i\frac{2\pi}{\lambda}n_1(\omega)d\right), \qquad (1)$$

in which $I(\omega)$ is the reference THz power signal and $O(\omega)$ is the signal passing through the sample after the fast Fourier

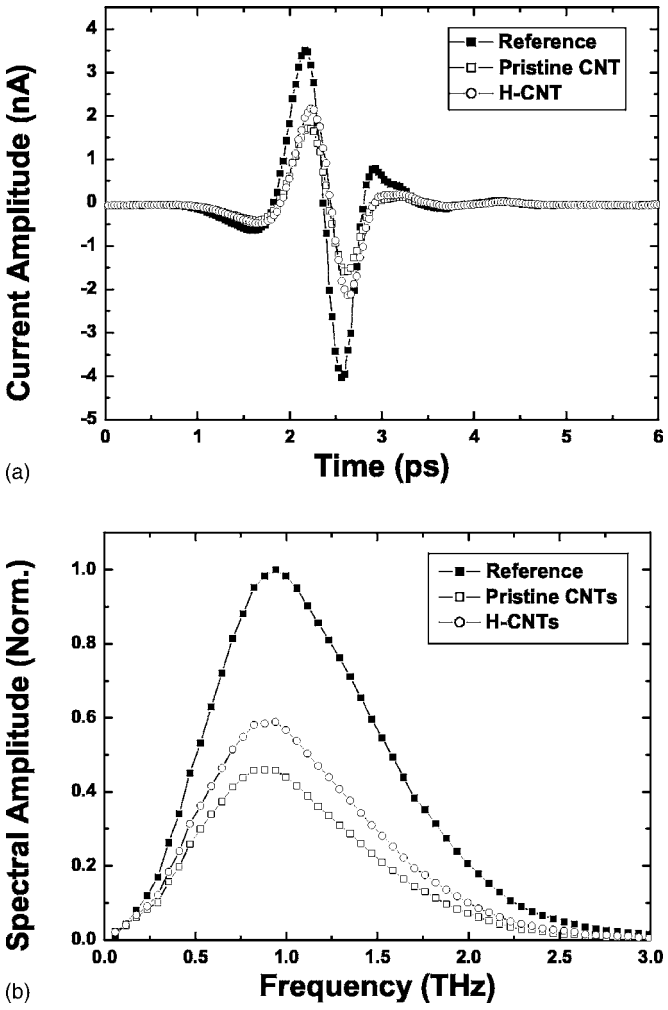


FIG. 2. (a) THz time-domain wave forms of the reference (closed squares), pristine carbon nanotubes (open squares), and hydrogen-functionalized carbon nanotubes (open circles); and (b) frequency-domain wave forms after fast Fourier transformations.

transformation. $\alpha(\omega)$ is the power absorption, $n_1(\omega)$ is the real part of the complex index of refraction, and $d$ is the film thickness. The imaginary index of refraction $n_2(\omega)$ is given by the power absorption $\alpha(\omega)=4\pi n_2/\lambda_0$.

The frequency-dependent complex dielectric constants and electrical conductivities can be deduced from the complex index of refraction. The frequency-dependent dielectric constant of the CNT film is described as follows:[16,19]

$$\varepsilon(\omega) = \varepsilon_{\mathrm{CNT}} + i\frac{\sigma}{\omega\varepsilon_0}, \qquad (2)$$

in which $\varepsilon_{\mathrm{CNT}}$ is the dielectric constant of the CNT at infinity, $\sigma$ is the conductivity, and $\varepsilon_0$ is the free space permittivity.

The optical constants and ac electrical conductivities of the pristine and hydrogenated CNTs are shown in Fig. 3. Figure 3(a) shows the power absorption spectra. The power absorptions of both samples increased with frequency. However, the power absorption of the hydrogen-functionalized CNTs was smaller than that of the pristine CNTs. Also, the difference in the absorptions of pristine and hydrogenated

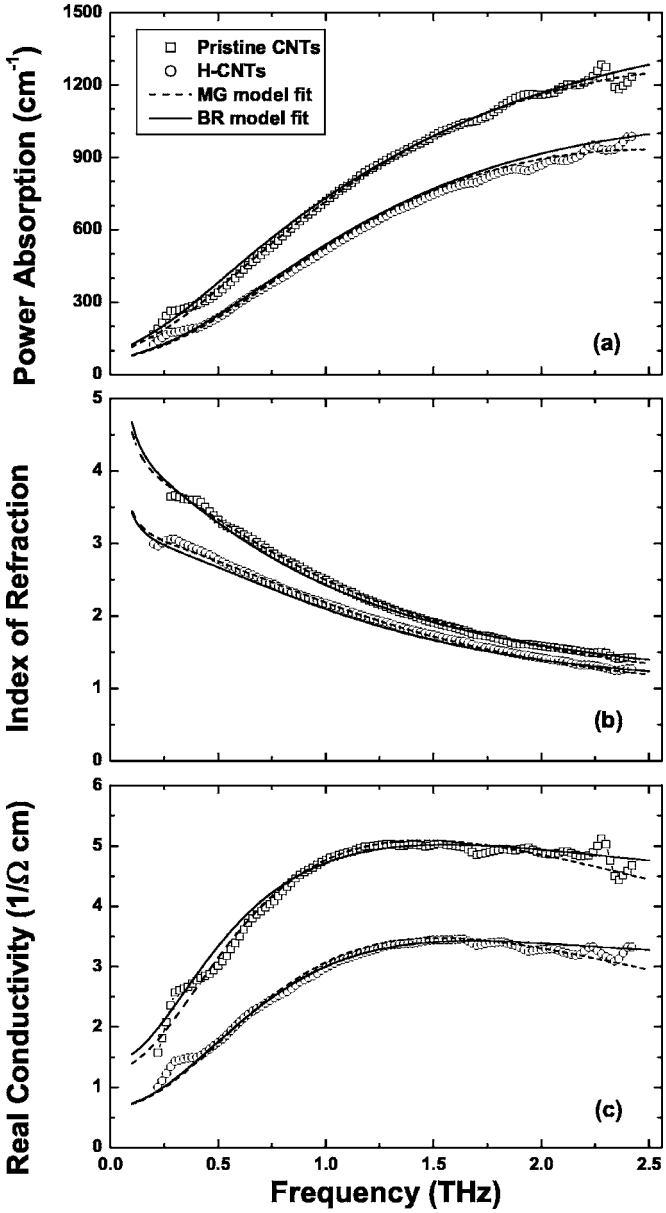


FIG. 3. Optical and electrical constants with fits of the Maxwell-Garnett (MG) and Bruggeman (BR) models. (a) Power absorption of the pristine carbon nanotubes (open square) and the hydrogen-functionalized carbon nanotubes (open circles); (b) indices of refraction; and (c) real conductivities. The dashed and solid lines are the MG and BR models, respectively.

CNTs was larger in the higher-frequency region. The power absorption can be used to estimate the change in the carrier density after hydrogen functionalization. The indices of refraction as functions of the frequency are shown in Fig. 3(b), which decreased in both samples with frequency increase. The magnitude of the refractive index of hydrogenated CNTs was smaller than that of pristine CNTs. The real conductivity is shown Fig. 3(c), which is proportional to the product of the power absorption and the real part of the refractive index $[\sigma(\omega)=c\alpha(\omega)n_1(\omega)\varepsilon_0]$. The real part of the conductivities of both samples started leveling off from 1.2 THz, as shown in Fig. 3(c). It is assumed from these broadenings that the phonon resonances of the CNTs are located in the THz region, because the graphite phonon resonance is in the few meV range.[20]. If the measurement range can be increased, the broadening peak range will be clearly shown. This is in good agreement with previous far-infrared spectroscopic measurements.[10] Real conductivities decreased by 20–40 % in this study's frequency range after hydrogen functionalization. As conductivity is proportional to carrier density, the reduction in the conductivity indicates that hydrogenation depleted the carriers.

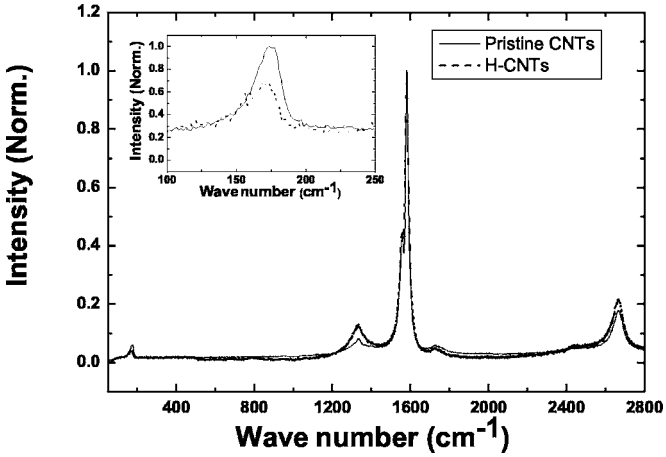


FIG. 4. Raman intensities of pristine carbon nanotubes (solid line) and hydrogen-functionalized carbon nanotubes (dashed line). Inset is the radial breathing mode.

To monitor chemical-bonding states and structural change, Raman spectroscopic measurements were performed with carbon nanotubes before and after the hydrogenation process and the results are shown in Fig. 4. Through Raman spectroscopy, the diameter characteristics in the 50–300 $cm^{-1}$ range were determined as the diameter is inversely proportional to the radial breathing mode, $\omega\ (cm^{-1})=239/[d\ (nm)]$, where $\omega$ is the radial frequency and $d$ is the diameter. Moreover, the D band (1380 $cm^{-1}$) and G band (1580 $cm^{-1}$) represent the states of $sp^3$ and $sp^2$ bonding that are related to dielectric and metallic properties, respectively.[20] The inset of Fig. 4 shows the radial breathing modes before and after hydrogen functionalization, with no change in peak position, whereas the ratio of $D$ and $G$ bands increased after hydrogenation. This implies that the carbon-hydrogen bonding rarely affects the structure of CNTs, but the bonding properties significantly change and the carbon-hydrogen bonding enhances the dielectric properties, which decreases conductivity. This is in good agreement with the results of the THz experiment.

A CNT bundle is an ensemble of tubes with various electronic structures, as the CNT was grown. In addition, regarding its electronic applications, understanding the network and link properties in CNTs is as essential as understanding single-CNT characteristics. Therefore, to study a CNT bundle, an analytical model, such as the effective medium approximation (EMA), that explains this composite system is necessary.[21–23] The EMAs used most commonly are the Maxwell-Garnett (MG) and the Bruggemann (BR) models, which are shown in Fig. 5.

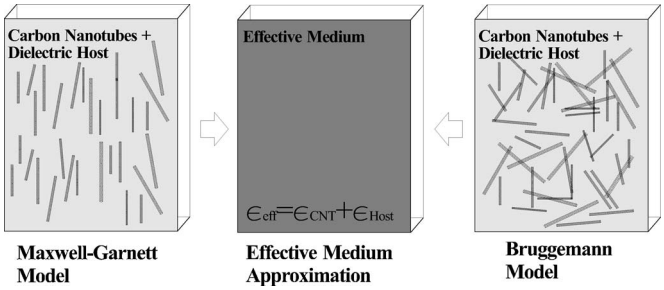


FIG. 5. Scheme of the Maxwell-Garnett model and Bruggemann models. See text for details.

Both models originated from the classical Clausius-Mossotii model, in which the polarized particle was embedded in a dielectric host material.[22] In the MG model, the distance between the polarized particles is significant. Thus, the interactions between the polarized particles are not taken into account. Instead, the MG model considers only the interactions between the polarized particles and the dielectric host. With the BR approximation, however, overlapping is assumed between the conductive and dielectric media, and interactions are considered between polarizing particles. Therefore, the BR model is more acceptable when the ratios of the metal particles are increased. To apply EMAs to experimental results, some conditions between the conducting particles and electromagnetic waves have to be satisfied. In general, the inclusion particles must be sufficiently smaller than the wavelength of electromagnetic waves so that the macroscopic Maxwell equation can be applied. Therefore, the experimental results of THz spectroscopy can be explained, as the CNTs are some micrometers long and the wavelength of the THz electromagnetic pulses is from several tens to a few hundreds of micrometers.

To ensure that the experimental results fitted the model values, the CNT films were assumed to consist of CNTs and air. The frequency-dependent dielectric function of CNTs, which consists of the Drude and Lorentz harmonic oscillator models, describes the case in this study, as shown by the following equation:

$$\varepsilon_{\mathrm{CNT}}(\omega) = \frac{-\omega_p^2}{\omega^2 + i\Gamma\omega} + \sum_i \frac{\omega_{p,i}^2}{(\omega_i^2 - \omega^2) - i\Gamma_i\omega} + \varepsilon_\infty, \quad (3)$$

in which $\omega_p$ is the plasma frequency, $\Gamma$ is the damping rate, $\omega_{p,i}$ is the oscillator strength of the Lorentz harmonic oscillator, $\omega_i$ is the phonon frequency, $\Gamma_i$ is the spectral width, and $\varepsilon_\infty$ is the dielectric constant at infinity.

The effective medium equations for the MG and BR models are as follows, respectively:[25]

$$f\frac{\varepsilon_{\mathrm{sub}} - \varepsilon_{\mathrm{CNT}}}{\varepsilon_{\mathrm{sub}} + 2\varepsilon_{\mathrm{CNT}}} = \frac{\varepsilon_{\mathrm{eff}} - \varepsilon_{\mathrm{CNT}}}{\varepsilon_{\mathrm{eff}} + 2\varepsilon_{\mathrm{CNT}}} \quad (4)$$

and

TABLE I. Fitting parameters (THz) of the Maxwell-Garnett and the Bruggemann models. $N=1/3$ is a geometrical factor, $\omega_p$ the plasma frequency, $\Gamma$ the damping rate, $\omega_{p,j}$ the oscillator strength of the Lorentz oscillators, $\omega_j$ the phonon frequency, and $\Gamma_j$ the spectral width.

| | | $\omega_p/2\pi$ | $\Gamma/2\pi$ | $\omega_{p,j}/2\pi$ | $\omega_j/2\pi$ | $\Gamma_j/2\pi$ | $f$ |
|---|---|---|---|---|---|---|---|
| CNTs | MG | 12.68 | 52.26 | 5.78 | 1.46 | 3.66 | 0.75 |
| | BG | 13.89 | 51.80 | 6.06 | 1.44 | 4.19 | 0.80 |
| H-CNTs | MG | 7.42 | 34.29 | 4.69 | 1.53 | 3.27 | 0.75 |
| | BG | 7.68 | 33.57 | 4.71 | 1.49 | 3.32 | 0.8 |

$$f\frac{\varepsilon_{\mathrm{sub}} - \varepsilon_{\mathrm{CNT}}}{\varepsilon_{\mathrm{sub}} + 2\varepsilon_{\mathrm{CNT}}} = (1-f)\frac{\varepsilon_{\mathrm{eff}} - \varepsilon_{\mathrm{CNT}}}{\varepsilon_{\mathrm{eff}} + 2\varepsilon_{\mathrm{CNT}}}, \quad (5)$$

in which $\varepsilon_{\mathrm{eff}}$ is the effective dielectric constant, $\varepsilon_{\mathrm{sub}}$ is the dielectric constant of the dielectric host, and $f$ is the filling factor of the CNTs in the dielectric host.

The experimental results were made to fit into both models. A geometrical factor of one-third was used because the CNTs were randomly aligned. An infinite dielectric constant of 3.24 was used. Through a scanning electronic microscope image, the filling factor was defined as over 0.6, and 0.75 and 0.8 were used for the MG and BR models, respectively. The fitting results of both models are shown in Fig. 3. The dashed lines represent the fitting data for the MG model, whereas the solid lines are the fitting data for the BR model. The fitting parameters are shown in Table I. The models have similar values. The plasma frequency in the fitting results was reduced to two-thirds of its original value after hydrogen functionalization, and the other fitting parameters were also reduced, except for the phonon frequency. The phonon frequencies of both model fits agree well with that of the graphite.[24] As the square of the plasma frequency is proportional to the carrier density, the plasma frequency reduction indicates the reduction of the carrier density in the CNTs after hydrogen functionalization, which also explains the decrease in conductivity.

The plasma frequencies in our results, obtained through the EMAs, do not agree with the plasmons of a single CNT, such as the $\pi$ (a few eV) and $\sigma$ (a few tens of eV) plasmons, although the results of this study have similar values to those from microwave spectroscopy.[2,11] The differences between the plasmon of a single CNT and the values in this study are assumed to be due to the reactance of the CNT networks, as samples in this study were composed of many networks. It was shown in Ref. 25 that the resistivity of the CNT networks increased when junctions were formed. The rise in reactance reduced network mobility in the CNT film by the order of three or four after networks and junctions were bunched up. As shown in Table I, damping rates of both samples also appeared in the THz region. The damping rate is dependent on the inverse of the carrier lifetime, and recent experimental results show that the carrier lifetime is from subpicoseconds to a few picoseconds.[26,27]

## CONCLUSION

The frequency-dependent optical and electrical properties of hydrogen-functionalized CNTs were characterized using

THz time-domain spectroscopy for 0.2–2.5 THz. Reduction of the magnitude of the power absorption and the refractive index after hydrogen functionalization was observed. The electrical conductivity was, therefore, reduced. Using Raman spectroscopy to monitor structural and chemical properties, the ratio of the *D* and *G* bands was found to increase after hydrogenation, which means that the dielectric property increased, which is in good agreement with the THz experimental results. To analyze the experimental results, effective medium approximations such as the MG and BR models were used. The effective plasma frequencies obtained from the approximations were in the THz region, which is due to the reactance increment in the CNT networks. Reductions in plasma frequencies and damping rates were also observed after hydrogen functionalization. Consequently, the plasma frequency reduction implies a decrease in the carrier density, because the carrier density is proportional to the square of the plasma frequency.

## ACKNOWLEDGMENT

This work was supported by Grant No. KRF-2004-015-C00175 of the Korea Research Foundation.

*Present address: Advanced Photonic Research Institute, Gwangju Institute of Science & Technology, 1 Oryong-dong, Buk-gu, Gwangju 500-712, Korea.

†Corresponding author. Electronic address: joohiuk@uos.ac.kr

[1] S. Iijima, Nature (London) **354**, 56 (1991).

[2] M. S. Dresselhaus, G. Dresselhaus, and Ph. Avouris, *Carbon Nanotubes: Synthesis, Structure, and Applications* (Springer, New York, 2000).

[3] Z. Yao, H. W. Ch. Postma, L. Balents, and C. Dekker, Nature (London) **402**, 273 (1999).

[4] S. J. Tans, A. R. M. Verschueren, and C. Dekker, Nature (London) **393**, 49 (1998).

[5] P. Avouris, Chem. Phys. **281**, 429 (2002).

[6] X. Zheng, G. H. Chen, Z. Li, S. Deng, and N. Xu, Phys. Rev. Lett. **92**, 106803 (2004).

[7] Y. Zhou, A. Gaur, S.-H. Hur, C. Kocabas, M. A. Meitl, M. Shim, and J. A. Rogers, Nano Lett. **4**, 2031 (2004).

[8] K. S. Kim, D. J. Bae, J. R. Kim, K. A. Park, S. C. Lim, J-.J. Kim, W. B. Choi, C. Y. Park, and Y. H. Lee, Adv. Mater. (Weinheim, Ger.) **14**, 1818 (2002).

[9] J. H. Lee, H. Kim, S.-J. Kahng, G. Kim, Y.-W. Son, J. Ihm, H. Kato, Z. W. Wang, T. Okazaki, H. Shinohara, and Y. Kuk, Nature (London) **415**, 1005 (2002).

[10] A. Ugawa, A. G. Rinzler, and D. B. Tanner, Phys. Rev. B **60**, R11305 (1999).

[11] O. Hilt, H. B. Brom, and M. Ahlskog, Phys. Rev. B **61**, R5129 (2000).

[12] A. Moussenssan, M. C. Wanke, Y. J. Li, J.-C. Chiao, S. J. Allen, T. W. Crowe, and D. B. Rutlege, IEEE Trans. Microwave Theory Tech. **46**, 1976 (1998).

[13] R. Köhler, A. Tredicucci, F. Beltram, H. E. Beere, E. H. Linfield, A. G. Davies, D. A. Ritchie, R. C. Iotti, and F. Rossi, Nature (London) **417**, 156 (2002).

[14] D. Grischkowsky, S. Keiding, M. van Exter, and Ch. Fattinger, J. Opt. Soc. Am. B **7**, 2006 (1990).

[15] T.-I. Jeon, K.-J. Kim, C. Kang, S.-J. Oh, J.-H. Son, K. H. An, D. J. Bae, and Y. H. Lee, Appl. Phys. Lett. **80**, 3403 (2002).

[16] T.-I. Jeon, K.-J. Kim, C. Kang, I.-H. Maeng, J.-H. Son, K. H. An, D. J. Bae, and Y. H. Lee, J. Appl. Phys. **95**, 5736 (2004).

[17] J.-H. Son, W. Sha, J. Kim, T. B. Norris, J. F. Whitaker, and G. A. Mourou, Appl. Phys. Lett. **63**, 923 (1993).

[18] J.-H. Son, T. B. Norris, and J. F. Whitaker, J. Opt. Soc. Am. B **11**, 2519 (1994).

[19] C. Kang, I. H. Maeng, S. J. Oh, J.-H. Son, T.-I. Jeon, K. H. An, S. C. Lim, and Y. H. Lee, Appl. Phys. Lett. **87**, 041908 (2005).

[20] M. S. Dresselhaus, G. Dresselhaus, A. Jorio, A. G. Souza Filho, and R. Saito, Carbon **40**, 2043 (2002).

[21] K. Tanaka, T. Yamabe, and K. Fukui, *Science and Technology of Carbon Nanotubes* (Elsevier, Amsterdam, 1999).

[22] *Electrical Transport and Optical Properties of Inhomogeneous Media*, edited by J. C. Garland and D. B. Tanner, AIP Conf. Proc., No. 40 (AIP, New York, 1978).

[23] J. S. Ahn, K. H. Kim, T. W. Noh, D.-H. Riu, K.-H. Boo, and H.-E. Kim, Phys. Rev. B **52**, 15244 (1995).

[24] Ch. Simon, F. Batallan, I. Rosenman, H. Lauter, and G. Furdin, Phys. Rev. B **27**, 5088 (1983).

[25] L. Hu, D. S. Hecht, and G. Gruner, Nano Lett. **4**, 2513 (2004).

[26] J.-S. Lauret, C. Voisin, G. Cassabois, C. Delalande, P. H. Roussignol, O. Jost, and L. Capes, Phys. Rev. Lett. **90**, 057404 (2003).

[27] O. J. Korovyanko, C.-X. Sheng, Z. V. Vardeny, A. B. Dalton, and R. H. Baughman, Phys. Rev. Lett. **92**, 017403 (2004).